Open-loop control of liquid-crystal spatial light modulators for vertical atmospheric turbulence wavefront correction

Chao Liu,[1,2] Lifa Hu,[1] Quanquan Mu,[1] Zhaoliang Cao,[1] and Li Xuan[1,*]

[1]State Key Laboratory of Applied Optics, Changchun Institute of Optics, Fine Mechanics and Physics, Chinese Academy of Sciences, Changchun, Jilin 130033, China

[2]Graduate School of the Chinese Academy of Sciences, Beijing 100039, China

*Corresponding author: xuanli@ciomp.ac.cn

Received 11 August 2010; revised 10 November 2010; accepted 10 November 2010; posted 11 November 2010 (Doc. ID 133221); published 27 December 2010

We present an open-loop adaptive optics (AO) system based on two liquid-crystal spatial light modulators (LCSLMs) that profit from high precision wavefront generation and good repeatability. A wide optical bandwidth of 300 nm is designed for the system, and a new open-loop optical layout is invented to conveniently switch between the open and closed loop. The corresponding control algorithm is introduced with a loop frequency (the reciprocal of the total time delay of a correction loop) of 103 Hz. The system was mounted onto a 2.16 m telescope for vertical atmospheric turbulence correction. The full width at half-maximum of the image of the star α Boo reached 0.636 arc sec after the open-loop correction, while it was 2.12 arc sec before the correction. The result indicates that the open-loop AO system based on LCSLMs potentially has the ability to be used for general astronomical applications.

OCIS codes: 010.1080, 230.3720, 010.1330.

1. Introduction

Deformable mirror (DM) devices have been widely used as wavefront correctors in a variety of adaptive optics (AO) systems [1–7]. Because of the hysteresis and mechanical coupling between adjacent actuators of the DM, it cannot acquire a highly accurate correction in one correction step. Therefore, the closed-loop control must be used to make the whole system work stably and accurately [8]. Although the closed-loop control may be suitable for some systems, it also has some problems when it is used on extremely large telescopes and multiobject AO systems [9]. In addition, it makes the whole system complex and not very fast. However, for an open-loop system, it only requires a single image to capture the control signal of the DM instead of several required by a closed-loop system, thereby increasing the bandwidth. Thus, open-loop control of a DM is currently being researched [8,10,11].

In recent years, liquid-crystal spatial light modulators (LCSLMs) have become increasingly attractive for use as wavefront correctors in AO systems [12–15]. These devices have many advantages as wavefront correctors, such as a large number of pixels, compactness, light weight, low power, low cost, and programmability, as demonstrated by many researchers [16–18]. More importantly, they have good repeatability and linearity [19], and they have been shown to have high precision in generating a desired wavefront [12,20,21], which makes the open-loop control possible.

The main drawback with the liquid-crystal (LC) device for wavefront correction is its polarization dependence, which means that it can only modulate 50% of the incident unpolarized light. To solve this problem, several methods have been proposed by

0003-6935/11/010082-08$15.00/0

others [22–25]. But it makes the devices or AO systems hard to manufacture and expensive. However, in an open-loop optical layout, the problem can be solved easily. The nonmodulated part of the incident light is used for wavefront sensing, and the modulated part is used for imaging [19,26].

Traditional LC AO systems are under closed-loop control [17,27–32]. With the benefit of feedback, it is easy to achieve highly accurate compensation, although the correction frame rate (the reciprocal of the time interval between the starting points of two adjacent correction loops) is not very fast. Cao *et al.* have demonstrated the possibility of using this kind of system to correct weak horizontal turbulence [31]. However, due to the low temporal bandwidth, the closed-loop system can only partially correct the vertical atmospheric turbulence [32]. Dayton *et al.* used a faster dual frequency LCSLM in a closed-loop AO system to observe a low Earth orbit satellite [17]. Because of the high driving voltages of the dual-frequency LCSLM, it is difficult to manufacture with millions of active pixels. Mu *et al.* have designed an open-loop LC AO system to correct horizontal turbulence, and they have acquired nearly diffraction-limited-resolution images [26]. However, to the best of our knowledge, use of an open-loop LC AO system to correct distortion in the vertical path of atmospheric turbulence has not been reported until now.

The purpose of this research is to evaluate the performance of an open-loop AO system based on LCSLMs for the vertical atmospheric turbulence correction. The system designs are introduced in Section 2. Section 3 presents the measurement of the interaction matrices (IMs) and control algorithm. The field experiment is introduced in Section 4. Finally, the conclusion follows in Section 5.

2. Open-Loop System Designs

A. Design of the Wide Optical Band

An inherent limitation of a LC-based AO system is the chromatic dispersion of the LC material. This limits the optical bandwidth to no more than 100 or 200 nm [33,34]. Therefore, we divide the visible light spectrum into two subspectra (600 to 700 nm and 700 to 900 nm) and compensate them independently to save the incident light energy, as shown in Fig. 1. First, we choose two liquid-crystal-on-silicon (LCOS, a kind of LCSLM) devices with central wavelengths of 633 (LCOS633) and 785 nm (LCOS785), respectively. Second, a color film (CF_1) is used to transmit the light from 600 to 900 nm. Then, the light is split into two beams by another color film (CF_2). The reflected beam from 600 to 700 nm goes into LCOS633. The transmitted beam from 700 to 900 nm goes into LCOS785. Third, the two beams are compensated and reflected back by the corresponding LCOSs, respectively. Finally, the two corrected beams are combined together for imaging.

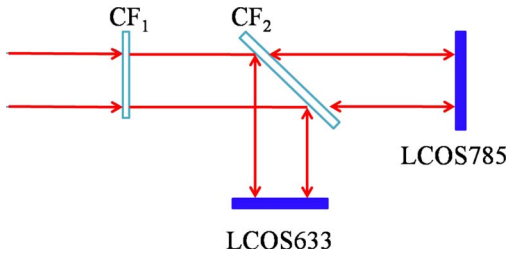

Fig. 1. (Color online) Schematic diagram of splitting the light by spectral content and compensating each separately: CF1 and CF2, color films; LCOS633 and LCOS785, LCOS devices.

B. Design of a New Open-Loop Optical Layout

For a conventional LC open-loop system [see Fig. 2(a)] [26], the incident unpolarized light is split into two orthogonal polarization beams by a polarizing beam splitter (PBS). One beam, whose polarization direction is parallel to the LC alignment direction, is used for compensation. The other beam is used for wavefront sensing. In this configuration, the LCOS actions cannot be detected by the wavefront sensor (WFS). When the open-loop system needs to measure the interaction matrix (IM) [35], it needs help from a subsystem that makes it become a closed-loop configuration [26], which makes the AO system more complicated and may introduce extra wavefront aberrations. In addition, the WFS and LCOS are located in different optical paths. This may introduce the non-common-path error.

To solve these problems, a new open-loop system is invented [see Fig. 2(c)]. The PBS is positioned behind the LCOS. The incident unpolarized light that strikes the LCOS can be divided into two components with orthogonal polarization directions. One component whose polarization direction is parallel to the LC alignment direction can be modulated by the LCOS. Then it is reflected by the PBS and used for imaging. The other component, which cannot

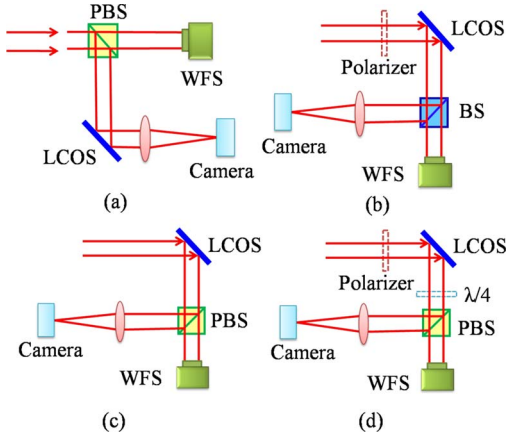

Fig. 2. (Color online) Schematic diagrams of open- and closed-loop optical systems: (a) conventional open-loop optical system, (b) conventional closed-loop optical system, (c) a new open-loop optical system, (d) new closed-loop optical system. PBS, polarizing beam splitter; BS, nonpolarizing beam splitter; WFS, wavefront sensor; $\lambda/4$, quarter-wave plate.

be modulated by the LCOS, is transmitted through the PBS and used for wavefront sensing. It should be emphasized that this system is an open-loop system, although it very much looks like a closed-loop configuration [see Fig. 2(b)]. When the open-loop AO system needs to measure the IM, only a polarizer and a quarter-wave plate are needed to make it become a closed-loop configuration [see Fig. 2(d)]. First, the polarizer is inserted before the LCOS, and it transmits a linearly polarized light, which has a polarization direction parallel to the LC alignment direction. Then, the light is modulated and reflected by the LCOS. Third, a quarter-wave plate is inserted before the PBS and changes the modulated light into a circularly polarized light. Finally, the PBS divides the circularly polarized light into two orthogonal polarization beams, both of which have been modulated by the LCOS. In this case, the WFS can detect the actions of the LCOS, and the IM can be measured conveniently. In addition, the WFS and the LCOS are located in the same optical path. The non-common-path error does not exist in the system.

C. Open-Loop Optical Layout for Vertical Turbulence Wavefront Correction

Based on the designs mentioned above, the optical layout of an open-loop AO system for vertical turbulence correction is designed and shown in Fig. 3. After the beam from the telescope goes through the color film CF_1, it is collimated by a lens L_1 (focal length $f_1 = 75$ cm) and reflected by a tip–tilt mirror (TTM). The reflected light is magnified by a beam expanding system composed of lenses L_2 ($f_2 = 65$ cm) and L_3 ($f_3 = 27$ cm). The magnified beam is divided into two beams by the color film CF_2, and each goes into a corresponding LCOS with a small incident angle (less than 2.5°). After the two beams are corrected and reflected back by their corresponding LCOSs, they are combined together. Then, the combined light goes through another beam expanding system composed of lenses L_3 and L_4 ($f_4 = 9$ cm). The PBS divides it into two orthogonal polarization beams. The transmitted nonmodulated beam goes into the WFS. The reflected modulated beam goes into a science camera. It must be noted that the two LCOSs are optically conjugated with the TTM, the telescope entrance pupil, and the lenslets of the WFS. Because of the open-loop configuration, the residual error cannot be detected by the WFS when the correction is in process. The image quality after correction is the main criterion of system performance.

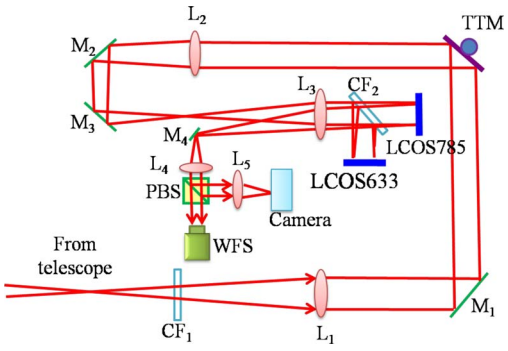

Fig. 3. (Color online) Optical layout for an open-loop AO system: L_1–L_5, lenses; M_1–M_4, mirrors; TTM, tip–tilt mirror.

3. Interaction Matrix Measurement and Control Algorithm

A. Interaction Matrix Measurement

Open-loop systems are simple and stable, but they must be very accurately calibrated because any uncertainty or disturbance can greatly affect the accuracy of the systems. The WFS has 400 hexangular lenslets. The average Fried parameter r_0 of the observatory was considered as 9 cm for a wavelength of 633 nm when designed for the AO system. Therefore, only a 1.8 m diameter segment of the 2.16 m telescope aperture was designed for the system $[(D/r_0)^2 = (1.8/0.09)^2 = 400]$. Each LCOS has 256 × 256 pixels. The pixel resolution is so high that the wavefront compensation error due to the finite corrector-element size can be neglected. In this case, each subaperture of the WFS subtends roughly 163 pixels on the LCSLM (see Fig. 4). Based on this configuration, the Zernike modes [36] (only take the first 35 Zernike terms in our system, due to the limitation of calculating time), excluding the piston mode, are used to measure the IMs [35]. The optical layout for measuring the IM of LCOS633 is shown in Fig. 5. A fiber bundle of white source is positioned on the focus of the telescope. A polarizer and a quarter-wave plate are inserted into the system to make it become a closed-loop configuration, as mentioned in Subsection 2.B. It should be noted that the light reflected by LCOS785 must be blocked by a black screen when measuring the IM of LCOS633 (see Fig. 5). Similarly, the light reflected by LCOS633 must be blocked when measuring the IM of LCOS785.

When a set of commands, also called "gray map," of the jth Zernike mode [37] with a unit coefficient (means one wavelength) is sent to a LCOS to

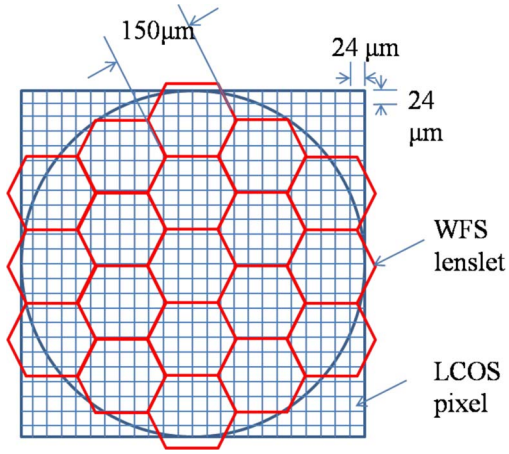

Fig. 4. (Color online) Schematic diagram of the arrangement of WFS lenslets with respect to the LCOS pixels.

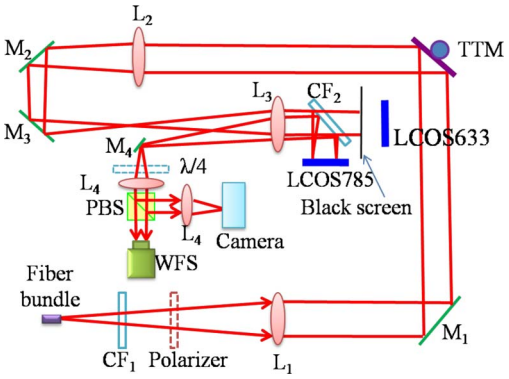

Fig. 5. (Color online) Optical layout of measuring the interaction matrix of LCOS633.

generate a corresponding wavefront φ_j, the slope vector of the wavefront, s_j, can be measured by the WFS:

$$s_j = [s_{1jx}, s_{2jy}, \cdots, s_{kjx}, s_{kjy}, \cdots, s_{Kjx}, s_{Kjy}]^T, \quad (1)$$

where (s_{kjx}, s_{kjy}) is the local average slope of the wavefront at the kth lenslet, and K is the total effective lenslets. Actually, s_j may contain some static errors introduced by the optical system and background. In our experiment, the errors have been measured and eliminated. Repeating this process to all J Zernike modes selected, The IM can be constructed:

$$\mathrm{IM} = [s_1, \cdots, s_j, \cdots, s_J]. \quad (2)$$

This method can be used to measure the IMs of LCOS633 (IM_{633}) and LCOS785 (IM_{785}).

The IM of the TTM ($\mathrm{IM}_{\mathrm{TTM}}$) also needs to be measured. The TTM has two orthogonal axes and one actuator for each. After a unit voltage is applied on one of the actuators, a corresponding wavefront is generated, and its slope vector can be measured by the WFS. The corresponding global tip–tilt vector $\bar{s}$ can be calculated by

$$\bar{s}_x = \left(\sum_{k=1}^{K} s_{kx}\right)/K, \qquad \bar{s}_y = \left(\sum_{k=1}^{K} s_{ky}\right)/K,$$
$$\bar{s} = [\bar{s}_x, \bar{s}_y]^T, \quad (3)$$

where (s_{kx}, s_{ky}) is the local average slope of the wavefront at the kth lenslet of the WFS. The global tip–tilt vector $\bar{s}$ is saved in a column of the $\mathrm{IM}_{\mathrm{TTM}}$. Repeating this procedure to the other actuator, the $\mathrm{IM}_{\mathrm{TTM}}$ can be constructed.

B. Control Algorithm

The slope vector of an aberrated wavefront, s, measured by the WFS can be expressed as

$$s = [s_{1x}, s_{1y}, \cdots, s_{kx}, s_{ky}, \cdots, s_{Kx}, s_{Ky}]. \quad (4)$$

It can be divided into two components: the global tip–tilt component and the remaining component. The global tip–tilt component is corrected by the TTM, and the remaining component is corrected by the LCOSs. The global tip–tilt can be calculated through Eq. (3), and the command vector for the TTM is

$$v = \mathrm{IM}_{\mathrm{TTM}}^{-1}\bar{s},$$

where $\mathrm{IM}_{\mathrm{TTM}}^{-1}$ is the inverse matrix of $\mathrm{IM}_{\mathrm{TTM}}$. Because of the fact that the TTM is always in a closed-loop configuration (see Fig. 6), the command vector for each correction loop is

$$V^{(n)} = V^{(n-1)} - k_G \cdot v, \quad (6)$$

where n is the number of iterations and k_G is a closed-loop proportion factor varying from 0 to 1.

The remaining component of the slope vector can be calculated by subtracting the global tip–tilt component

$$s' = [(s_{1x} - \bar{s}_x), (s_{1y} - \bar{s}_y), \cdots, (s_{kx} - \bar{s}_x), (s_{ky} - \bar{s}_y), \cdots (s_{Kx} - \bar{s}_x), (s_{Ky} - \bar{s}_y)]^T. \quad (7)$$

Then, the gray map, gm, of the LCOS can be calculated by

$$c = \mathrm{IM}^{+}s', \qquad \psi = \sum_{i=1}^{J} c_i Z_i, \qquad \mathrm{gm} = \mathrm{mod}(-\psi), \quad (8)$$

where IM^{+} is the pseudoinverse matrix of the IM, c is a reconstructed Zernike coefficient vector with the unit of wavelength, c_i is the ith element of c, ψ is the reconstructed wavefront with the unit of wavelength and dimension of 256×256, Z_i is the ith Zernike polynomial [37], and $\mathrm{mod}(\cdot)$ means modulo one operation, as the unit of ψ is wavelength. Using IM_{633} and IM_{785} to replace IM in Eq. (8), we can acquire the gray maps of LCOS633 (gm_{633}) and LCOS785 (gm_{785}), which can be sent to corresponding LCOSs directly to correct the aberrated wavefront, respectively (see Fig. 6).

4. Open-Loop Correction of Vertical Turbulence Wavefront

The 2.16 m reflecting telescope is located at Xinglong Station of the Beijing Astronomical Observatory. Figure 7 shows a photograph of the telescope and its optical diagram. The diameter of the primary mirror A, in Fig. 7(a), is 2.16 meters. It has a Cassegrain focus F_1 and a Coudé focus F_2. We used several

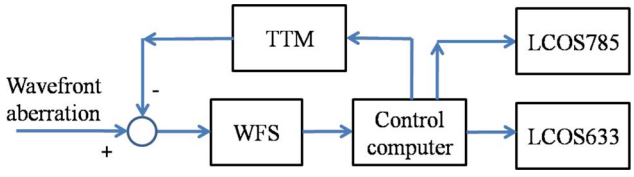

Fig. 6. (Color online) Block diagram of the control system for correcting the vertical turbulence wavefront.

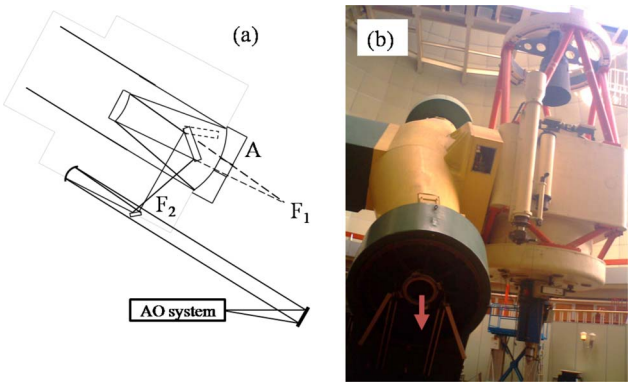

Fig. 7. (Color online) Representation of the 2.16 m telescope located at Xinglong Station of Beijing Astronomy Observatory: (a) optical diagram and (b) photograph of the telescope.

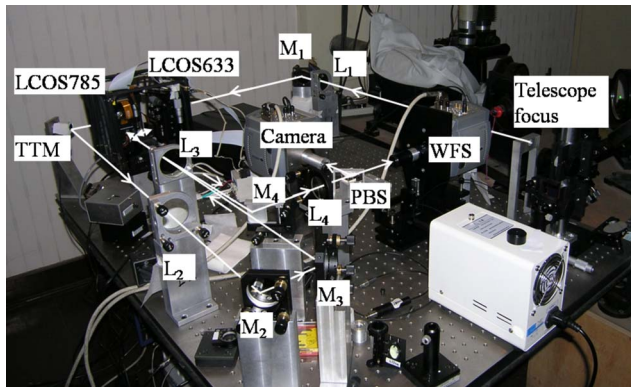

Fig. 9. (Color online) Experimental layout of the open-loop AO system based on LCOSs.

mirrors to relay the light from the telescope to the AO system, as shown in Fig. 8(a). A stop was placed at a pupil image of the telescope aperture so that only light from a 1.8 m diameter segment was used. The double LCOSs were aligned carefully [see Fig. 8(b)], and they were wrapped by a thermostat that maintained the temperature of the LCOSs at 37 °C. Figure 9 shows the experimental layout of the open-loop AO system. LCOS633 and LCOS785 are from Boulder Nonlinear Systems (BNS) Company, USA, with a response time of 3.5 and 4.5 ms, respectively. The WFS is a ShaH 1000 Shack–Hartmann WFS from Visionica, Ltd., Russia, with a sampling frequency of 500 Hz. The TTM is a S330 TTM from Piezo Nano Positioning (PI) Company, Germany. The science camera is a DU 897 CCD from Andor, Ltd., Northern Ireland.

A correction loop includes several steps. First, the WFS collects light and reads out the data. Then, the control computer begins to calculate a set of commands for the TTM and a gray map for each LCOS. Third, these sets of commands are sent to corresponding devices in parallel. Finally, after the transmission of gray maps is complete, a time of 4.5 ms is added to wait for the response of the LCOSs. The time series of a correction loop includes data collecting time (4 ms), calculating time (0.8 ms), transmission time (0.4 ms), and response time (4.5 ms). The total delay time of a correction loop is 9.7 ms. Therefore, the loop frequency (the reciprocal of total time delay of a correction loop) is 103 Hz (1/9.7 ms). For the open-loop operation mode, the AO system can be controlled with a consecutive or concurrent mode, as the open-loop control is a no-feedback system. For the consecutive control mode, the next correction loop starts when the present loop has finished. The correction frame rate (the reciprocal of the time interval between the starting points of two adjacent correction loops) is equal to the loop frequency. In order to increase the 3 dB temporal bandwidth of the system, the concurrent mode [38] was considered. In this case, the next loop will be starting while the present loop has not finished yet; then, the correction frame rate is much larger than the loop frequency. To obtain the largest correction frame rate, the time interval between the starting points of two adjacent loops should be the longest delay segment [38]. The LC response time of 4.5 ms is the longest delay segment in our system. Therefore, the maximum correction frame rate of 222 Hz (1/4.5 ms) can be achieved.

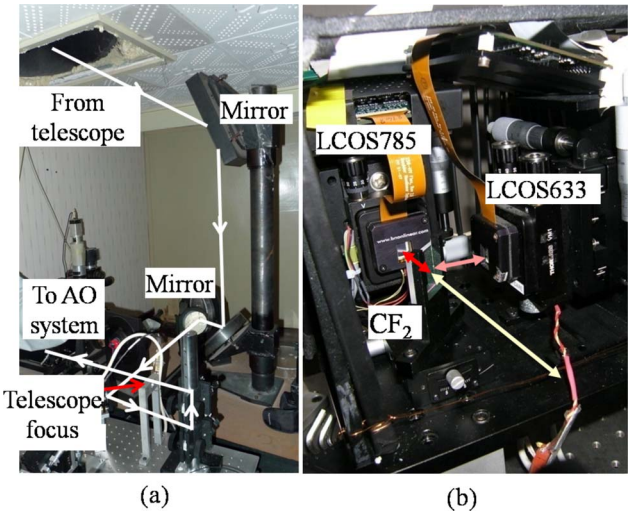

Fig. 8. (Color online) (a) Connection of the optical setup between the telescope and AO system; (b) detailed diagram of the double LCOSs.

At midnight of 22 April 2010, the star α Boo was tracked by the 2.16 m telescope. In order to know the condition of the turbulence during observation, we measured the Fried parameters r_0 with the WFS. The slopes of the two lenslets, which have an interval of two lenslets, are used to calculate r_0 by the theory of differential image motion measurements (DIMM) [39]. The Fried parameter r_0 was about 8 cm at 633 nm (see Fig. 10), which was a little smaller than the 9 cm that has been considered when designing the AO systems. Therefore, the ratio of the effective telescope aperture to the Fried parameter, $D/r_0(1.8/0.08)$, was equal to 22.5, which indicates that the uncompensated resolution was far from a diffraction-limited resolution.

Figure 11 illustrates the images of the star α Boo before and after correction with a 30 ms exposure

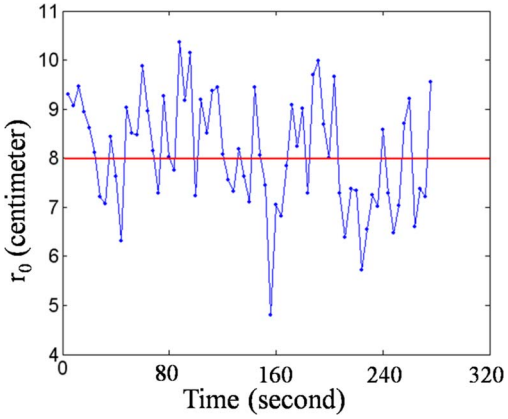

Fig. 10. (Color online) Fried parameter r_0 measured on 23 April 2010 in Xinglong Station of Beijing Astronomy Observatory. The zero of the time axis (start time) is 01:37:02 (Beijing time).

time. Before correction, the full width at half-maximum (FWHM) of the image of α Boo was 2.12 arc sec. After correction, it decreased to 0.636 arc sec, which was only 30% of that before correction. The Strehl ratio was estimated by computing the ratio of the peak intensity in the images to what would be expected if the images were diffraction limited. After correction, the Strehl ratio was 0.12, while it was 0.02 before correction. The movie with AO off and on is shown in Fig. 11(b).

The diffraction-limited resolution of the telescope is 0.11 arc sec at 780 nm. Although the angular resolution and Strehl ratio of the star image after correction were improved a lot, they were still far from the diffraction-limited resolution. There were several reasons for this. First, the ratio D/r_0 of 22.5 was a little larger than the 20 lenslets across the telescope pupil, which was probably not enough to get the most accurate wavefront measurements. Second, the temporal bandwidth of our LC AO system was relatively low. Because of the long response time of LCOS785, the temporal bandwidth, $f_{3\,\mathrm{dB}}$, of our open-loop AO system was only about 17 Hz. The average wind speed measured by the observatory was 1.5 m/s, and the Fried parameter was 8 cm during our measurements. The corresponding Greenwood frequency, f_G, at the observatory was about 27.2 Hz at our optical band of 600–900 nm. The temporal error could be calculated by

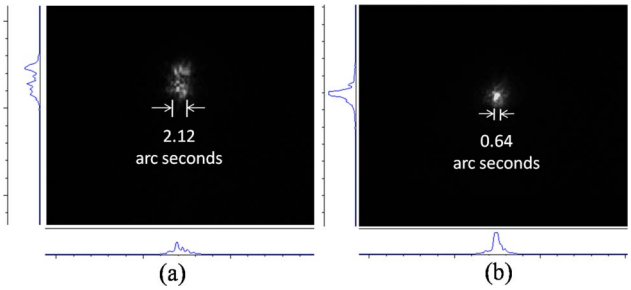

Fig. 11. (Color online) Images of star α Boo captured with a CCD camera with an exposure time of 30 ms: (a) without correction and (b) with the open-loop correction (Media 1).

$$\sigma^2 = (f_G/f_{3\,\mathrm{dB}})^{5/3},$$

which reached 2.2 rad^2. Finally, due to the limitation of calculating time, only 35 Zernike modes excluding the piston were used to expand the turbulence wavefront. The expansion residual error could be calculated by $0.2944 \times J^{-\sqrt{3}/2}(D/r_0)^{5/3}$ [40], where J was the number of Zernike modes used, and the error equaled 2.3 rad^2. Therefore, more Zernike modes (e.g., 90 modes, and the corresponding expansion error is only 1 rad^2) have to be used to decrease the expansion error in the future.

To increase the temporal bandwidth of the AO system, faster LCOSs with a response time of less than 2 ms have been under fabrication by our group recently. If these new devices could be used in the open-loop system, its correction frame rate would exceed 500 Hz. We estimate that the corresponding temporal bandwidth $f_{3\,\mathrm{dB}}$ of the system would reach 25 Hz. In this case, the temporal error of the AO system would decrease to 1.1 rad^2. In this case, the quality of the image would be much better.

Another method to increase the image quality is to use the near-infrared light with an optical band of 700–1000 nm for imaging. As the Greenwood frequency is proportional to $\lambda^{-6/5}$, the turbulence speed will decrease in this optical band, which benefits system performance.

5. Conclusion

In summary, we have demonstrated an open-loop AO system based on double LCOS wavefront correctors that profit from high-precision wavefront generation and good repeatability. Past work on the open-loop LC AO systems has concentrated on laboratory measurement [19] and horizontal turbulence correction [26]. The experiment described in this paper was performed using the system in conjunction with the 2.16 m reflecting telescope located at Xinglong Station of the Beijing Astronomical Observatory. We believe that this is the first time that the open-loop LC AO system has been used to correct the vertical atmospheric turbulence. The advantages of the open-loop LC AO systems over corresponding closed-loop systems are polarization independence, faster speed, and simple operation.

Our open-loop system has the following two characteristics. First, a broad optical band of 300 nm is designed. We divide the light by spectral content and compensate each, separately. The optical band after being expanded is from 600 to 900 nm. Second, the open-loop optical layout is different from a conventional one. It is a very clever way to switch between an open and closed loop, which is beneficial for the measurement of IMs. In addition, the system does not suffer from the non-common-path error.

The real-time, field experiment showed that, the FWHM of the image of the star α Boo could reach 0.636 arc sec after the open-loop correction, while it was 2.12 arc sec before correction. After correction, the Strehl ratio reached 0.12, while it was

0.02 before correction. These results indicate that the open-loop AO system based on LCSLMs potentially has the ability to correct vertical atmosphere turbulence.

Because of the limited number of lenslets of the WFS, we only used a 1.8 m diameter segment of the 2.16 m telescope aperture. The diffraction-limited resolution of the corresponding effective aperture of the telescope was 0.11 arc sec at 780 nm. It indicates that the system was still in a low-order correction regime. Therefore, the system modification is required, particularly with the LC devices, in order to use the system for general astronomical applications.

The main limitation of the LCOSs is their long response time, which may decrease the temporal bandwidth of the AO systems. The response times of the LCOSs under fabrication by our group recently have been less than 2 ms. However, with continued improvements to the LC materials, the prospect of even shorter response times is promising.

We are grateful for assistance from the Xinglong Station of the Beijing Astronomy Observatory for the operation of the 2.16 m telescope. This work is supported by the National Natural Science Foundation of China (NSFC) (grants 60736042, 60578035, 50703039, and 60811120025). The authors also gratefully acknowledge the efforts and suggestions of all the referees.

References

1. P. Kern, P. Lena, P. Gigan, F. Rigaut, G. Rousset, J. C. Fontanella, J. P. Gaffard, C. Boyer, P. Jagourel, and F. Merkle, "Adaptive optics prototype system for infrared astronomy. 1. system description," Proc. SPIE **1271**, 243–251 (1990).
2. H. Takami, N. Takato, M. Otsubo, T. Kanzawa, Y. Kamata, K. Nakashima, and M. Iye, "Adaptive optics system for Cassegrain focus of Subaru 8.2 m telescope," Proc. SPIE **3353**, 500–507 (1998).
3. W. H. Jiang, G. M. Tang, M. Q. Li, N. Ling, C. H. Rao, C. L. Guan, L. T. Jiang, F. Shen, M. Li, Y. Y. Li, and D. H. Chen, "21-element infrared adaptive optics system at 2.16 m telescope," Proc. SPIE **3762**, 142–149 (1999).
4. A. Iriarte, S. Cuevas, J. E. Graves, and M. Northcott, "Adaptive secondary for the 2.1 m Telescope at SPM Observatory," Proc. SPIE **4007**, 537–546 (2000).
5. A. V. Larichev, P. V. Ivanov, N. G. Iroshnikov, V. I. Shmalhauzen, and L. J. Otten, "Adaptive system for eye-fundus imaging," Quantum Electron. **32**, 902–908 (2002).
6. M. A. van Dam, D. Le Mignant, and B. A. Macintosh, "Performance of the Keck Observatory adaptive-optics system," Appl. Opt. **43**, 5458–5467 (2004).
7. M. Vorontsov, J. Riker, G. Carhart, V. S. Gudimetla, L. Beresnev, T. Weyrauch, and L. C. Roberts, Jr., "Deep turbulence effects compensation experiments with a cascaded adaptive optics system using a 3.63 m telescope," Appl. Opt. **48**, A47–57 (2009).
8. K. Morzinski, K. Harpse, D. Gavel, and S. Ammons, "The open-loop control of MEMS: modeling and experimental results," Proc. SPIE **6467**, 64670G (2007).
9. D. T. Gavel, "Adaptive optics control strategies for extremely large telescopes," Proc. SPIE **4494**, 215–220 (2002).
10. C. Vogel and Q. Yang, "Modeling, simulation, and open-loop control of a continuous facesheet MEMS deformable mirror," J. Opt. Soc. Am. A **23**, 1074–1081 (2006).
11. J. Stewart, A. Diouf, Y. Zhou, and T. Bifano, "Open-loop control of a MEMS deformable mirror for large-amplitude wavefront control," J. Opt. Soc. Am. A **24**, 3827–3833 (2007).
12. G. Love, "Wave-front correction and production of Zernike modes with a liquid-crystal spatial light modulator," Appl. Opt. **36**, 1517–1520 (1997).
13. M. A. Neil, M. J. Booth, and T. Wilson, "Closed-loop aberration correction by use of a modal Zernike wave-front sensor," Opt. Lett. **25**, 1083–1085 (2000).
14. D. Dayton, S. Browne, J. Gonglewski, and S. Restaino, "Characterization and control of a multielement dual-frequency liquid-crystal device for high-speed adaptive optical wave-front correction," Appl. Opt. **40**, 2345–2355 (2001).
15. S. R. Restaino, D. M. Payne, J. T. Baker, J. R. Andrews, S. W. Teare, G. C. Gilbreath, D. Dayton, and J. Gonglewski, "Liquid crystal technology for adaptive optics: an update," Proc. SPIE **5003**, 187–192 (2003).
16. N. Collings, W. Crossland, P. Ayliffe, D. Vass, and I. Underwood, "Evolutionary development of advanced liquid crystal spatial light modulators," Appl. Opt. **28**, 4740–4747 (1989).
17. D. Dayton, J. Gonglewski, S. Restaino, J. Martin, J. Phillips, M. Hartman, P. Kervin, J. Snodgress, S. Browne, and N. Heimann, "Demonstration of new technology MEMS and liquid crystal adaptive optics on bright astronomical objects and satellites," Opt. Express **10**, 1508–1519 (2002).
18. L. Hu, L. Xuan, Y. Liu, Z. Cao, D. Li, and Q. Mu, "Phase-only liquid crystal spatial light modulator for wavefront correction with high precision," Opt. Express **12**, 6403–6409 (2004).
19. C. Li, M. Xia, Q. Mu, B. Jiang, L. Xuan, and Z. Cao, "High-precision open-loop adaptive optics system based on LC-SLM," Opt. Express **17**, 10774–10781 (2009).
20. P. Prieto, E. Fernandez, S. Manzanera, and P. Artal, "Adaptive optics with a programmable phase modulator: applications in the human eye," Opt. Express **12**, 4059–4071 (2004).
21. J. Schmidt, M. Goda, and B. Duncan, "Aberration production using a high-resolution liquid-crystal spatial light modulator," Appl. Opt. **46**, 2423–2433 (2007).
22. G. Love, "Liquid-crystal phase modulator for unpolarized light," Appl. Opt. **32**, 2222–2223 (1993).
23. T. L. Kelly and G. D. Love, "White-light performance of a polarization-independent liquid-crystal phase modulator," Appl. Opt. **38**, 1986–1989 (1999).
24. L. Hu, X. Li, Q. Mu, Z. Cao, D. Li, Y. Liu, Z. Peng, and X. Lu, "A polarization independent liquid crystal adaptive optics system," J. Opt. **12**, 045501 (2010).
25. D. Cai, J. Yao, and W. Jiang, "Liquid crystal adaptive optics system for unpolarized light," Proc. SPIE **7209**, 72090P (2009).
26. Q. Mu, Z. Cao, D. Li, L. Hu, and L. Xuan, "Open-loop correction of horizontal turbulence: system design and result," Appl. Opt. **47**, 4297–4301 (2008).
27. R. Dou and M. Giles, "Closed-loop adaptive-optics system with a liquid-crystal television as a phase retarder," Opt. Lett. **20**, 1583–1585 (1995).
28. J. Gourlay, G. Love, P. Birch, R. Sharples, and A. Purvis, "A real-time closed-loop liquid crystal adaptive optics system: first results," Opt. Commun. **137**, 17–21 (1997).
29. S. Restaino, D. Dayton, S. Browne, J. Gonglewski, J. Baker, S. Rogers, S. McDermott, J. Gallegos, and M. Shilko, "On the use of dual frequency nematic material for adaptive optics systems: first results of a closed-loop experiment," Opt. Express **6**, 2–6 (2000).
30. M. K. Giles, A. J. Seward, and T. M. Giles, "Closed-loop phase-contrast adaptive optics system using liquid crystal phase modulators: experimental results," Proc. SPIE **4493**, 174–183 (2002).

31. Z. Cao, Q. Mu, L. Hu, D. Li, Y. Liu, L. Jin, and L. Xuan, "Correction of horizontal turbulence with nematic liquid crystal wavefront corrector," Opt. Express **16**, 7006–7013 (2008).
32. Z. Cao, Q. Mu, L. Hu, D. Li, Z. Peng, Y. Liu, and L. Xuan, "Preliminary use of nematic liquid crystal adaptive optics with a 2.16-meter reflecting telescope," Opt. Express **17**, 2530–2537 (2009).
33. M. Gruneisen, R. Dymale, J. Rotgé, L. DeSandre, and D. Lubin, "Wavelength-dependent characteristics of a telescope system with diffractive wavefront compensation," Opt. Eng. **44**, 068002 (2005).
34. M. Gruneisen, R. Dymale, and M. Garvin, "Wavelength-dependent characteristics of modulo $N\lambda_0$ optical wavefront control," Appl. Opt. **45**, 4075–4083 (2006).
35. C. Boyer, V. Michau, and G. Rousset, "Adaptive optics: interaction matrix measurements and real time control algorithms for the Come-On project," Proc. SPIE **1542**, 46–61 (1991).
36. D. Miller, L. Thibos, and X. Hong, "Requirements for segmented correctors for diffraction-limited performance in the human eye," Opt. Express **13**, 275–289 (2005).
37. L. Thibos, R. Applegate, J. Schwiegerling, and R. Webb, "Standards for reporting the optical aberrations of eyes," J. Refract. Surg. **18**, 652–660 (2002).
38. Z. Cao, Q. Mu, L. Hu, Y. Liu, and L. Xuan, "Improve the loop frequency of liquid crystal adaptive optics by concurrent control technique," Opt. Commun. **283**, 946–950 (2010).
39. M. Sarazin and F. Roddier, "The ESO differential image motion monitor," Astron. Astrophys. **227**, 294–300 (1990).
40. R. J. Noll, "Zernike polynomials and atmospheric turbulence," J. Opt. Soc. Am. **66**, 207–211 (1976).